ORNL/TM-12294/V1

OAK RIDGE
NATIONAL
LABORATORY

LOCKHEED MARTIN

MANAGED AND OPERATED BY
LOCKHEED MARTIN ENERGY RESEARCH CORPORATION
FOR THE UNITED STATES
DEPARTMENT OF ENERGY

ORNL-27 (3-96)

SCALE-4 Analysis of Pressurized Water Reactor Critical Configurations: Volume 1 — Summary

M. D. DeHart

ORNL/TM-12294/V1

Computational Physics and Engineering Division

SCALE-4 ANALYSIS OF PRESSURIZED WATER REACTOR CRITICAL CONFIGURATIONS: VOLUME 1 — SUMMARY

M. D. DeHart

Date Completed: January 1995
Date Published: March 1995

Prepared under the direction of
Sandia National Laboratories
under Memorandum Purchase Orders 66-0162 and AD-4072
with Oak Ridge National Laboratory

Prepared by the
OAK RIDGE NATIONAL LABORATORY
managed by
MARTIN MARIETTA ENERGY SYSTEMS, INC.
for the
U.S. DEPARTMENT OF ENERGY
under contract DE-AC05-84OR21400

CONTENTS

LIST OF FIGURES

LIST OF TABLES

ABSTRACT

The requirements of ANSI/ANS 8.1 specify that calculational methods for away-from-reactor criticality safety analyses be validated against experimental measurements. If credit is to be taken for the reduced reactivity of burned or spent fuel relative to its original "fresh" composition, it is necessary to benchmark computational methods used in determining such reactivity worth against spent fuel reactivity measurements. This report summarizes a portion of the ongoing effort to benchmark away-from-reactor criticality analysis methods using critical configurations from commercial pressurized- water reactors (PWR).

The analysis methodology utilized for all calculations in this report is based on the modules and data associated with the SCALE-4 code system. Isotopic densities for spent fuel assemblies in the core were calculated using the SAS2H analytical sequence in SCALE-4. The sources of data and the procedures for deriving SAS2H input parameters are described in detail. The SNIKR code sequence was used to extract the necessary isotopic densities from SAS2H results and to provide the data in the format required for SCALE-4 criticality analysis modules. The CSASN analytical sequence in SCALE-4 was used to perform resonance processing of cross sections. The KENO V.a module of SCALE-4 was used to calculate the effective multiplication factor (k_{eff}) for the critical configuration. The SCALE-4 27-group burnup library containing ENDF/B-IV (actinides) and ENDF/B-V (fission products) data was used for analysis of each critical configuration.

Each of the five volumes comprising this report provides an overview of the methodology applied. Subsequent volumes also describe in detail the approach taken in performing criticality calculations for these PWR configurations: Volume 2 describes criticality calculations for the Tennessee Valley Authority's Sequoyah Unit 2 reactor for Cycle 3; Volume 3 documents the analysis of Virginia Power's Surry Unit 1 reactor for the Cycle 2 core; Volume 4 documents the calculations performed based on GPU Nuclear Corporation's Three Mile Island Unit 1 Cycle 5 core; and, lastly, Volume 5 describes the analysis of Virginia Power's North Anna Unit 1 Cycle 5 core. Each of the reactor-specific volumes provides the details of calculations performed to determine the effective multiplication factor for each reactor core for one or more critical configurations using the SCALE-4 system; these results are summarized in this volume. Differences between the core designs and their possible impact on the criticality calculations are also discussed. Finally, results are presented for additional analyses performed to verify that solutions were sufficiently converged. All calculations show the ability to predict a k_{eff} value very close to 1.0 for various conditions and cooling times. Thus, the methodology applied is shown to be a valid approach for calculating the value of k_{eff} for systems with spent PWR fuel.

1. INTRODUCTION

In the past, criticality analysis of pressurized-water-reactor (PWR) fuel in storage or transport has assumed that the fuel is fresh with the maximum allowable initial enrichment. This assumption has led to the design of widely spaced and/or highly poisoned storage and transport arrays. If credit is assumed for fuel burnup, more compact and economical arrays can be designed. Such reliance on the reduced reactivity of spent fuel for criticality control is referred to as "burnup credit." If burnup credit is applied in the design of a cask for use in the transport of spent light-water-reactor (LWR) fuel to a repository, a significant reduction both in the cost of transport and in the risk to the public can be realized.[1] These benefits caused the U.S. Department of Energy (DOE) to initiate a program to investigate the technical issues associated with burnup credit in spent fuel cask design. These efforts have been led by Sandia National Laboratories (SNL) and carried out as part of the Cask Systems Development Program within the Office of Civilian Radioactive Waste Management. This five-volume report documents work performed at Oak Ridge National Laboratory (ORNL) as part of a larger effort to demonstrate an acceptable approach for validating computational tools to be used in burnup credit cask design.

The computational tools of interest for burnup credit cask design are initially those currently used and accepted for spent fuel characterization (prediction of isotopics) and criticality safety (prediction of the effective multiplication factor, k_{eff}) in away-from-reactor (AFR) applications. The criticality analysis tools accepted for fresh fuel cask design have typically been validated per the requirements of the ANSI/ANS-8.1 criticality safety standard[2] (i.e., comparison against experimental data). Numerous critical experiments for fresh PWR-type fuel in storage and transport configurations exist and can be used as part of a validation data base. However, there are no critical experiments with burned PWR-type fuel in storage and transport configurations that can be directly used to extend the data base to the realm of burned fuel. Thus, as part of the effort to extend the validation of existing criticality analysis tools to the domain of burned fuel, it was decided to investigate the performance of AFR analysis methods in the prediction of measured reactor critical configurations. While elements of a reactor critical analysis do not directly correspond to analyses of spent fuel assemblies in transportation and storage casks (e.g., elevated temperatures in reactor configurations or poison plates in cask designs), comparison against measured critical configurations can be used to validate aspects of spent fuel cask configurations which are not addressed in other experiments (i.e., fission-product interactions and the prediction of time-dependent actinide and fission-product inventories). Reactor critical configurations contain a diverse range of nuclides, including fissile and fertile actinides, fission products, and activation products. Thus, nuclear reactor core criticals can be used to test the ability of an analysis methodology to generate accurate burned fuel isotopics and handle the reactivity effects of complex heterogeneous systems containing burned fuel.

This report describes the data and procedures used to predict the multiplication factor for several measured critical core configurations using a select set of AFR analysis codes. The analyses were performed for precise state points at beginning of cycle (BOC) (mixture of fresh and burned fuel) and at measured state points throughout the cycle depletion (all burned fuel). Self-consistency among the reactor criticals in the prediction of k_{eff} will allow the determination of the bias of the approach taken in representing the effect of those materials not present in fresh fuel.

To date, the SCALE code system[3] developed at ORNL has been the primary computational tool used by DOE to investigate technical issues related to burnup credit.[4] SCALE is a well-established code system that has been widely used in AFR applications for spent fuel characterization via the SAS2H/ORIGEN-S analysis sequence[5] and criticality safety analyses via the CSAS/KENO V.a analysis sequence.[6] The isotopic composition of the spent fuel is derived from a SAS2H/ORIGEN-S calculation that simulates two-dimensional (2-D) effects in a one-dimensional (1-D) model of an LWR fuel assembly. The depletion model is a spatially independent point model using cross sections and neutron flux parameters derived from the 1-D fuel assembly model. The KENO V.a Monte Carlo code[7] is used to calculate the neutron multiplication factor for complex multidimensional systems. KENO V.a has a large degree of flexibility in its geometrical modeling capabilities that enables spent fuel arrays and container geometries to be modeled in explicit detail. The SCALE-4 27-group burnup library containing ENDF/B-IV (actinides) and ENDF/B-V (fission products) data was used for all calculations.

Early efforts to analyze reactor criticals[8] using the SCALE modules concentrated on using utility-generated isotopic data, although some analyses were performed using isotopics calculated with SAS2H. Based on this initial work, a consistent SCALE-based analysis methodology that simplifies both the data requirements and the calculational procedure was developed. The criteria used to select the reactor critical configurations were (1) applicability to the PWR fuel to be used in burnup credit cask design (e.g., long downtimes for decay of short-lived isotopes, large percentages of burned fuel in the configuration), the need to verify consistency in calculated results for different reactor conditions, and the need to provide a comparison with the results of ref. 8. Acceptable performance of the SCALE system in the prediction of k_{eff} will be judged relative to established SCALE performance for fresh fuel systems; if agreement is seen within the range typical for fresh fuel systems, then it will be concluded that the methodology described herein is valid in terms of its treatment of depletion and decay calculations and fission-product interactions, within the range of application defined by the reactor conditions.

The purpose of this volume of this report is to provide an overview of the reactor critical analyses that are described in detail in the subsequent volumes of this report. The ensuing sections of this volume will perform the following functions: (1) describe the methodology employed in reactor critical analyses for the reactor cores detailed in subsequent volumes, (2) summarize and compare the differences between reactor configurations and the results of the critical calculations for these configurations, (3) discuss sensitivity and convergence tests performed, (4) compare results to those obtained for benchmarks against LWR-type critical experiments, and (5) compare results to those of earlier scoping reactor critical analyses.

2. OVERVIEW OF THE REACTOR CRITICAL METHODOLOGY

The impetus for the analysis of reactor critical configurations is to validate a methodology similar to that used by a cask designer performing criticality analysis for spent fuel assemblies. To this end, a straightforward calculational strategy has been established that minimizes the data required to characterize the spent fuel. The remainder of this section provides a generalized description of the procedure applied in the analysis of three different reactor cores: Tennessee Valley Authority's Sequoyah Unit 2 (Cycle 3), Virginia Power's Surry Unit 1 (Cycle 2), GPU Nuclear Corporation's Three Mile Island Unit 1 (Cycle 5), and Virginia Power's North Anna Unit 1 (Cycle 5). The core designs of each of these three systems have peculiarities that must be accounted for in individual computational models. These aspects of the calculations are addressed in the detailed description of the individual calculations given in Vols. 2 through 5 of this report. The following description provides an overview of the shared features of the set of reactor critical calculations, without addressing the specifics of individual reactor designs.

The methodology applied in reactor critical analyses can be broken into five steps: (1) grouping of fuel assemblies into similar-content groups and similar-burnup subgroups; (2) calculation of burnup-dependent isotopics for each group; (3) interpolation of decay calculations from results of the previous step to obtain both individual assembly and subgroup isotopics; (4) cross-section processing based on subgroup isotopics; and (5) preparation of a KENO V.a model based on the actual core geometry, individual assembly isotopics, and subgroup-evaluated cross sections. The model developed in step 5 is used to calculate the effective multiplication factor, k_{eff}, for the reactor.

Figure 1 provides a graphical overview of these steps, showing the relationships between the data and codes used in each stage of the calculation. The first step shown in the figure represents the process of collecting assembly information from reactor documentation. Eighth-core symmetry is assumed to reduce the number of unique assembly models, such that the burnup of each assembly in an eighth-core segment represents the average burnup of all assemblies located in the corresponding symmetric position across the core. Using the reactor information, "groups" of assemblies are identified that are of cognate background (i.e., same initial loading and burn cycles). These assembly groups are then further categorized into "subgroups" consisting of assemblies within a group with similar (±2 GWd/MTU) burnups.

The second step shown in the figure involves the calculation of isotopic contents using the decay and depletion steps of the SAS2H calculational sequence of SCALE. Calculations are performed for each assembly group based on the initial fresh fuel content and operating history of the group. Output consists of calculated isotopic contents for each of a number of user-specified time steps.

In step 3, the SNIKR code package (not a part of the SCALE system) is used to interpolate between isotopics for appropriate time steps to obtain the assembly-specific isotopic contents for each assembly to be used in the KENO V.a core model. (SNIKR is a simple tool used to automate the task of extracting, interpolating, and formatting data; however, this process can be performed manually.) SNIKR is also used to calculate the isotopics for the average burnup of each assembly subgroup.

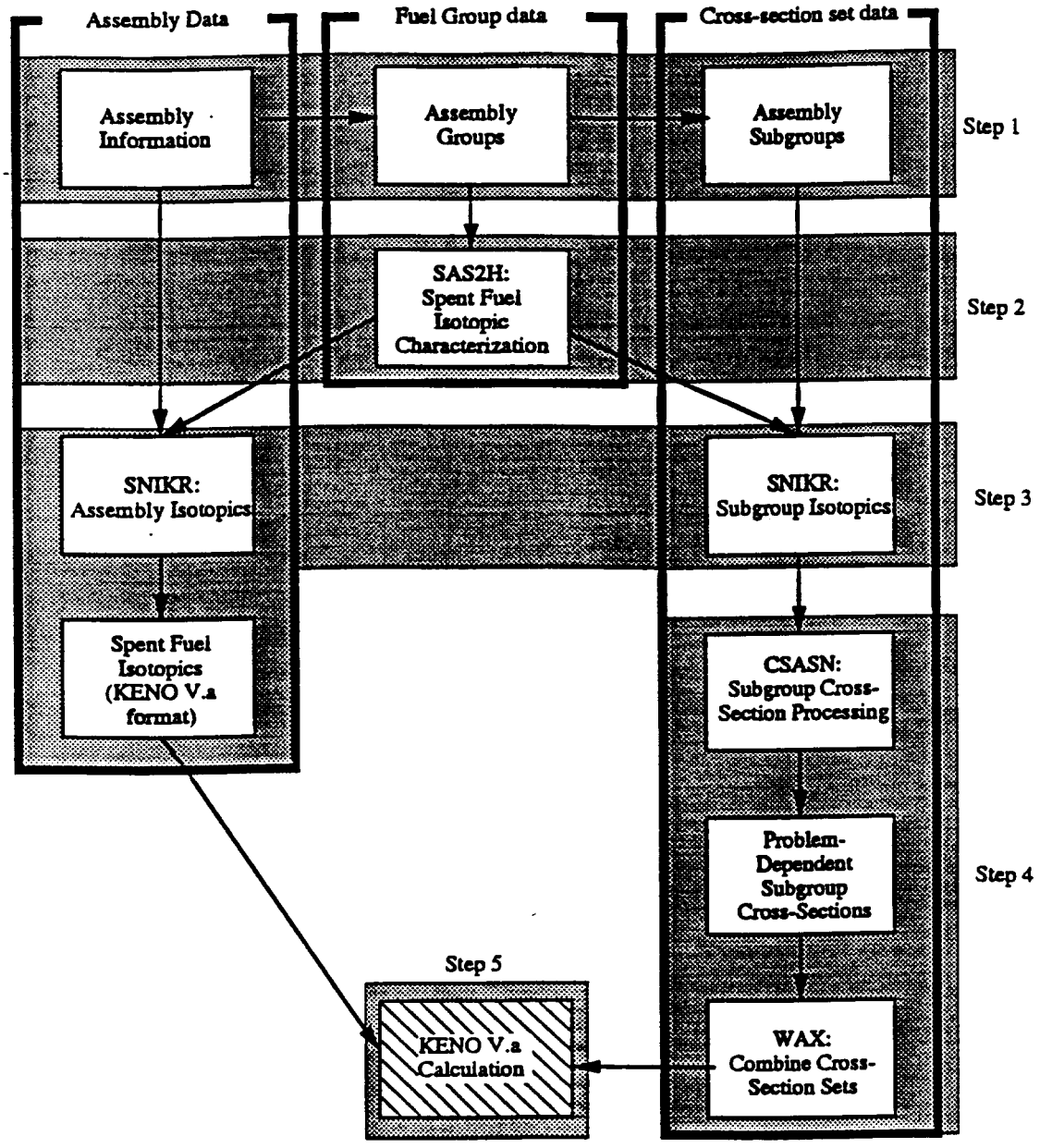

Fig. 1. Overview of the reactor critical calculation procedure.

The results of step 3 are used in step 4 to create fuel pin models based on the average composition of an assembly subgroup; the CSASN sequence in SCALE is then used to calculate the problem-dependent, group-weighted cross sections for each subgroup. The SCALE module WAX is then used to combine all subgroup-based cross sections into a single working library, where cross-section identifiers are assigned such that each numeric identifier indicates both a specific isotope and the subgroup upon which it was based.

Finally, in step 5 a KENO V.a model is created based on the core geometry, again assuming eighth-core symmetry. Thus, while a full-core model is prepared, each eighth-core segment of the core is identical in composition to the other eighth-core segments. (A full-core model in KENO V.a is more computationally efficient than an eighth-core model with reflective boundary conditions.) Fuel assemblies are assumed to be uniform in composition (all fuel pins are comprised of the same material), and isotopics are obtained from the burnup-specific results obtained in step 3. Assembly isotopes are assigned cross-section identifiers corresponding to the appropriate subgroup-based cross sections derived in step 4. Remaining core information is obtained from the reactor documentation. Calculations are then performed to determine the value of k_{eff} for the reactor model and to verify that the solution has converged.

The specifics of each of the steps described above are discussed in detail in each of the following sections.

2.1 FUEL ASSEMBLY GROUPS

Since many assemblies in a reactor begin with identical initial compositions and experience simultaneous operating histories, these similar fuel assemblies can be collected effectively into groups, with one depletion calculation performed for each group. It is assumed that at a given burnup, all assemblies within a group have the same isotopic content. If the isotopic content of a group is known as a function of burnup, then one can interpolate to obtain the specific isotopics for a given assembly burnup. This interpolation is discussed further in Sect. 2.3.

A minimum granularity for grouping is to collect fuel assemblies by reactor fuel batch. In the nomenclature generally applied by commercial PWR core designers, a fuel batch is typically comprised of a single enrichment fuel, all loaded at the same time, and all residing in-core for the same fuel cycles. Three fuel batches (i.e., enrichments) are usually present in the first operating cycle of a reactor. These batches are typically designated by the numbers 1, 2, and 3. Prior to each subsequent cycle of operation, one new batch of fuel is usually added and some of the depleted fuel assemblies are removed. Each new batch of fuel is assigned a unique identification number. If the new fuel assemblies to be loaded consist of more than one enrichment, they may be assigned as a "split batch," using the same number with a different letter appended to each enrichment (e.g., batches 4A and 4B could represent two different fuel enrichments loaded in a single cycle). Hence a given batch of assemblies has experienced identical operating periods, downtimes, and roughly the same power history, and thus meets the minimum requirements for a calculational fuel group. However, within a given fuel batch, additional fuel groups (i.e., separate depletion calculations) may be required when absorber materials [e.g., burnable poison rods (BPR) or control rods (CR)] are present in certain assemblies within the fuel batch or when core location is important.

As discussed earlier, it is possible to interpolate between a series of burnups within a given fuel group to determine the isotopic concentrations corresponding to a specific burnup. This interpolation procedure can be used to estimate the isotopic contents of each individual assembly in a fuel group. Based on these assembly isotopics, it is possible to generate a content-specific cross-section set for each assembly. However, since nuclide cross sections vary slowly with burnup, the analysis methodology can be simplified by preparing problem-dependent cross sections for a set of similar assemblies with similar burnups. Unfortunately, due to specific power variations related to the assembly locations in the core, it is possible to have a relatively wide range of burnups within a single fuel group. Thus, it may be necessary to divide fuel groups into subgroups based on burnup such that all assemblies included in a subgroup are within a limited burnup range; the number of subgroups will depend on the range of burnups contained in the fuel group. Calculations reported in Vols. 2 and 3 of this report indicate that fuel subgroups with burnup ranges of no more than 2 GWd/MTU can be adequately represented using cross sections generated based on the mean burnup of the subgroup's constituent assemblies.

2.2 DEPLETION CALCULATIONS

Depletion calculations are performed using the SAS2H sequence of the SCALE-4 code system and the 27-group burnup library. The SAS2H sequence invokes the ORIGEN-S[9] code to perform depletion and decay calculations. The SAS2H procedure also uses BONAMI[10] and NITAWL-II[11] for resonance processing followed by a 1-D two-part XSDRNPM spectrum calculation (part 1 is a pin-cell model; part 2 is an assembly model) at selected times in the irradiation history to generate burnup-dependent cross sections based on the given design and operating parameters. At the end of each burnup step, cross sections for default and any user-specified isotopes are recomputed using XSDRNPM based on the new isotopic composition. This process is illustrated in Fig. 2. The purpose of these calculations is to predict the isotopic content of each fuel group as a function of its operating history. If one or more fuel groups are comprised of fresh fuel at the time of the critical measurements, SAS2H calculations are not necessary for those groups; the isotopic content is based on that of the fresh fuel specifications.

Although it is important to model the presence of absorber rods [i.e., BPRs or CRs, (if present) for the cycle for which a criticality calculation is to be performed], experience has shown that the effect of such rods is diluted by later burn cycles with no absorber rods present. Thus, it is not necessary to model the history of the assembly with respect to the insertion and removal of absorber rods in earlier reactor cycles. The approach used in modeling absorber rods present in the current cycle will depend on the rod type and will vary between reactor designs. Further discussion of the treatment of such rods is included in each of the subsequent reactor-specific volumes of this report.

Since within a fuel group it is assumed that isotopic content is a function only of burnup, it is possible to calculate the content of the fuel at a given burnup by interpolation between SAS2H/ORIGEN-S isotopics provided at each burnup step. The manner of interpolation is discussed in the following subsection. SAS2H provides the capability to obtain the isotopic composition of a fuel assembly at specified burnup intervals given the initial composition of the fuel, clad, and moderator, design parameters of the fuel rod and lattice, and power history. To provide sufficient points for interpolation, the burnup history was divided into equal intervals of no more than 5 GWd/MTU. (This should not be confused with the 2-GWd/MTU interval used to establish

ORNL-DWG 94-12315

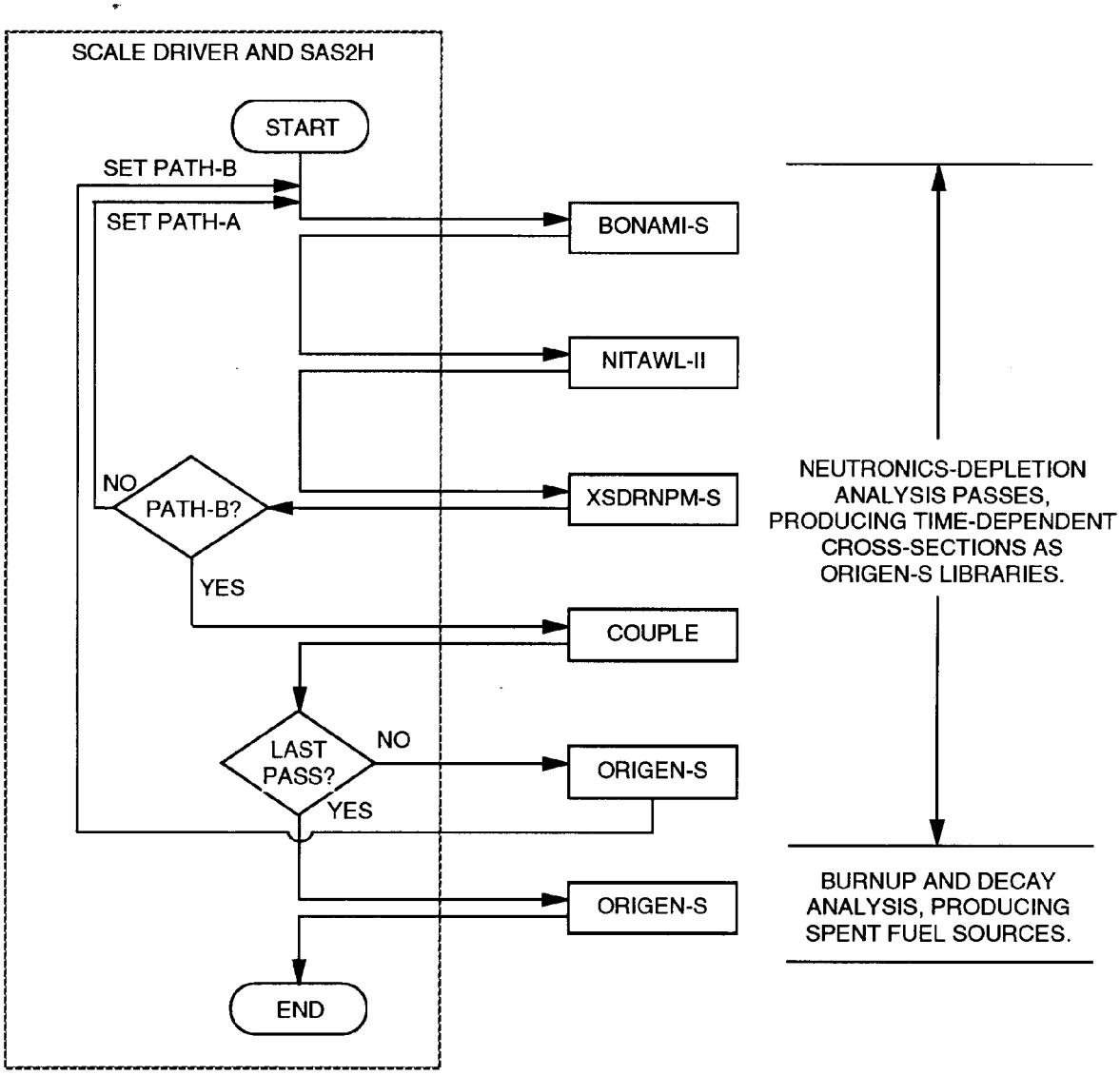

Fig. 2. Average energy group for fission for different assembly designs.

assembly subgroups. The 5-GWd/MTU interval represents an interpolation range over which isotopic concentrations are assumed to vary smoothly.) The fuel groups are depleted at least 1.2 times the maximum burnup (B_{max}) of the fuel group. Note that it is generally sufficient to calculate burnups out to the maximum burnup in a group, as this will bound all burnups in the group. A value of $1.2*B_{max}$ was used to allow the capability of modeling axial burnup variations where volume-averaged center region burnups may be up to 1.2 times larger than the assembly average. However, axial burnup variations are not included in the models presented in this report.

To make it possible to interpolate between burnup steps and account for downtime between cycles, a simplification is made in the burnup model. Since the burnup actually accumulated during each cycle varies for each fuel assembly in a group, a portion of the downtime was applied at the end of each burnup interval. This practice ensures that the spent fuel isotopics for all fuel assemblies contain the impact of the reactor cycle downtime when interpolation on burnup is performed. The ratio of uptime to downtime for each operating cycle is used to determine the downtime for each burnup interval. Average values for specific power are computed from the fuel group average burnups and the total uptime for the cycle. Isotopics for assembly-specific burnups may then be obtained via interpolation between calculated isotopics at the end of each burnup interval. This approach is illustrated in Fig. 3. The top portion of the figure shows the "actual" burnup histories for two hypothetical assemblies in a fuel group. Note that in this example the number of cycles and downtimes are the same, but that burnup in each assembly is different within each cycle. The lower portion of the figure demonstrates how the burnup of each assembly is represented in a SAS2H depletion, using a single calculation to represent the entire fuel group. Each cycle is broken down into multiple burnup intervals, each followed by a downtime (for the first two cycles). The final cycle is calculated with a sufficient number of burnup intervals to exceed the maximum burnup (31 MWd/MTU in Assembly A of Fig. 2) by 20%. The isotopics are then available at fixed time intervals, from which interpolation can be performed for assembly-specific burnups. Note that the burnup in each of the first two cycles is selected so as to represent average cycle burnups for the group. Any downtime between the end of the final burn cycle in the SAS2H model and the time of the subsequent reactor critical was not included in the SAS2H depletion, but it was explicitly modeled as described in Sect. 2.3.

As discussed earlier, group-weighted cross sections are calculated as a function of burnup within the SAS2H sequence using flux weighting performed by XSDRNPM for each specified burnup step. Cross sections are updated for a default set of isotopes built into the SAS2H sequence, plus any additional nuclides specified by the user. Table 1 shows the default set plus 44 additional actinides and fission products specified for reactor depletion cases. Also included is oxygen, which is present in significant quantities in UO_2 fuel. These nuclides represent a combination of the most important nuclides for burnup credit calculations and for reactor physics calculations. The selection of burnup credit nuclides is based on availability of experimentally measured isotopic concentrations and on sensitivity studies performed for a large number of nuclides under various spent fuel transportation/storage conditions, as described in ref. 12. The reactor physics nuclides are additional isotopes which are not important in a transportation sense, but have been determined to be important for depletion, decay, and criticality calculations under reactor operating conditions (e.g., ^{135}Xe builds in rapidly during reactor operation, but decays away with a 9.1-hour half-life, and is therefore unimportant in five-year cooled spent fuel). These nuclides were identified in earlier work.[13,14]

ORNL-DWG 94-12310

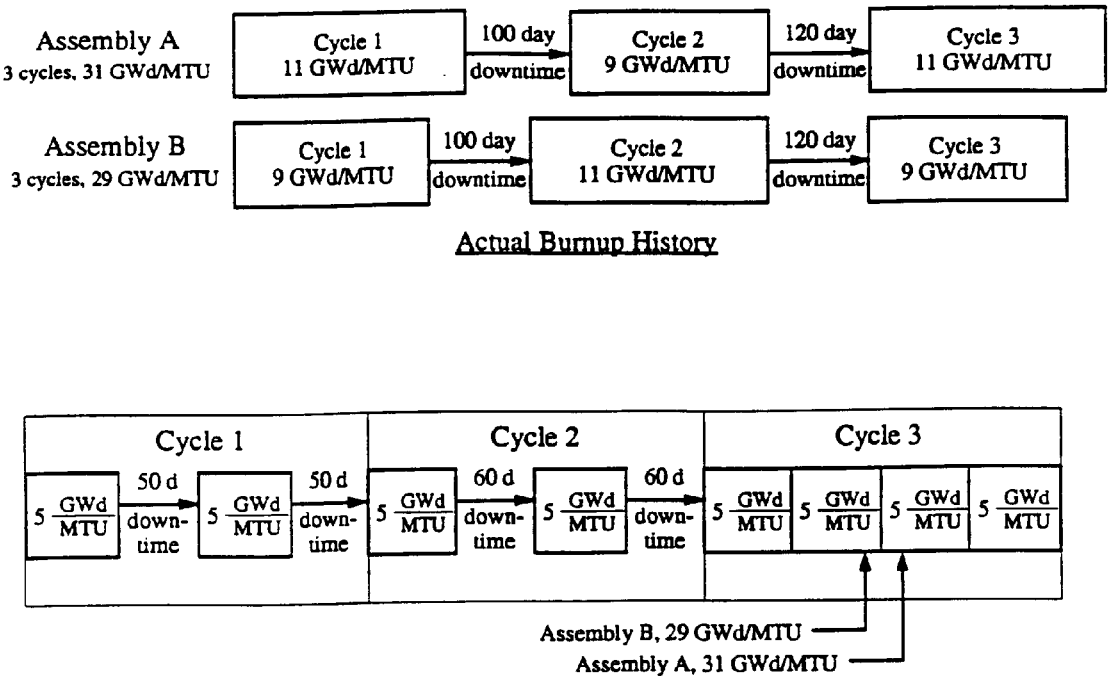

Fig. 3. SAS2H burnup model of assemblies within a fuel group.

Table 1. Nuclides updated by SAS2H

$^{234}U^{a}$	$^{243}Am^{a}$	^{94}Nb	^{132}Xe	^{145}Nd
$^{235}U^{a}$	$^{242}Cm^{a}$	$^{16}O^{b}$	$^{135}Xe^{a}$	^{147}Nd
$^{236}U^{a}$	$^{243}Cm^{a}$	^{99}Tc	^{136}Xe	^{147}Pm
$^{238}U^{a}$	$^{244}Cm^{a}$	^{101}Ru	$^{133}Cs^{a}$	^{148}Pm
$^{237}Np^{a}$	^{83}Kr	^{106}Ru	^{134}Cs	^{147}Sm
$^{238}Pu^{a}$	^{85}Kr	^{103}Rh	^{135}Cs	^{149}Sm
$^{239}Pu^{a}$	^{90}Sr	^{105}Rh	^{137}Cs	^{150}Sm
$^{240}Pu^{a}$	^{89}Y	^{105}Pd	^{136}Ba	^{151}Sm
$^{241}Pu^{a}$	^{95}Mo	^{108}Pd	^{139}La	^{152}Sm
$^{242}Pu^{a}$	^{93}Zr	^{109}Ag	^{144}Ce	^{153}Eu
$^{241}Am^{a}$	^{94}Zr	^{124}Sb	^{141}Pr	^{154}Eu
$^{242m}Am^{a}$	^{95}Zr	^{131}Xe	^{143}Pr	^{155}Eu
			^{143}Nd	^{155}Gd

[a]Automatically updated by SAS2H.
[b]Not an actinide or fission product, but present in UO_2 fuel.

Any additional cross sections required for depletion calculations are obtained from the more than 1000 nuclides available within the ORIGEN-S one-group LWR library and are adjusted with burnup using the ORIGEN-S spectral parameters (THERM, RES, and FAST)[15] using fluxes calculated by XSDRNPM. The ORIGEN-S one-group LWR library available in SCALE-4 has been updated to use cross sections from the SCALE-4 27-group burnup library for all 193 nuclides in that library, by extracting one-group cross sections from the output of a low-burnup, LWR-type fuel model using all burnup library nuclides as input.

Note that ORIGEN-S tracks all decay chains, and does not account for the loss of volatile isotopes; however, this is not felt to have a significant effect on isotopic calculations.

2.3 BURNUP-DEPENDENT NUCLIDE CONCENTRATIONS

As has been indicated in previous sections, the isotopic content at the end of the final burn cycle may be determined for each assembly or fuel subgroup by interpolating between burnups for which SAS2H/ORIGEN-S depletion calculations have been performed, based on the final burnup of the fuel. For a criticality condition obtained after the shutdown of the last cycle, it is necessary to perform decay calculations to account for the change in composition due to radioactive decay during the downtime prior to criticality.

The actual number densities used in the criticality calculations are derived from the SAS2H calculation for a given fuel batch using a newly developed interface module, SAS2H Nuclide Inventories for KENO Runs (SNIKR). (See Appendix C of Volumes 2, 3, and 5 and Appendix B of Vol. 4.) This module was developed to (1) automate the process of interpolation of number densities from a SAS2H calculation as a function of burnup, (2) perform the necessary decay calculations to

model cooling time for use in spent fuel critical calculations, and (3) print isotopic densities formatted in the form required for use in KENO V.a or CSAS calculations. Typically, the term "SNIKR" is used to refer to this three-step sequence of calculations; however, the package actually consists of two codes, SNIKR1 and SNIKR3, plus a driver script to execute the codes SNIKR1, ORIGEN-S, and SNIKR3 in sequence.

In the first phase of a SNIKR calculation, burnup-dependent nuclide inventories are read from a dataset produced from a SAS2H calculation. SNIKR1 uses a Lagrangian interpolation scheme to calculate nuclide concentrations for a specified burnup, where a polynomial of degree one less than the number of data points to be fit is used to represent the number density for each nuclide as a function of burnup. In the development of SNIKR, comparisons were made against results using nuclide concentrations calculated directly from SAS2H for a specified burnup to examine the effect of the interpolation procedure on pin-cell k_∞ (i.e., 1-D infinite-lattice calculation) values. The results of these comparisons indicated agreement to within 0.1% Δk in the k_∞ values calculated using isotopics derived from the two methods.[16]

Upon completing interpolation, SNIKR1 sets up the input needed to decay these burnup-specific isotopics to the requested cooling time using the ORIGEN-S point-depletion code. The second phase of SNIKR executes the ORIGEN-S module in the SCALE code system. Phase three of SNIKR reads the number densities produced by ORIGEN-S for the requested cooling time and extracts the nuclides to be used in the depleted fuel for the burnup credit criticality analysis. Number densities for these nuclides are then written to output files in the SCALE standard composition input format and the KENO V.a mixing table data format for use in CSAS and KENO V.a calculations, respectively.

SNIKR extracts concentrations for the set of nuclides specified by the user. The set of nuclides selected for the reactor critical benchmark calculations consists of the 48 nuclides listed in Table 2. These nuclides are a subset of those in Table 1, with the exception of ^{103}Ru, ^{135}I, ^{148}Nd, and ^{149}Pm. The cross sections of these four nuclides are small enough or change slowly enough with burnup that omitting them from the cross-section update in SAS2H has a negligible effect and are therefore not needed in the SAS2H calculation. In addition to the 25 nuclides selected for use in the burnup credit analysis in ref. 4, the list in Table 2 includes the other nuclides included in an earlier burnup credit feasibility study[1] together with nuclides modeled explicitly in the burnup credit work of refs. 13 and 14.

2.4 SUBGROUP CROSS-SECTION PROCESSING

The CSASN[6] sequence of the SCALE system is used to compute problem-dependent fuel pin cross sections based on the isotopic content and geometry of a lattice fuel cell. Based on a 1-D fuel pin model, CSASN invokes BONAMI-S[10] to perform resonance shielding calculations using Bondarenko factors, followed by NITAWL-II[11] calculations to perform resolved resonance range cross-section processing using the Nordheim Integral Treatment.

CSASN cross-section processing is applied only to subgroup-averaged nuclide concentrations. As discussed earlier in Sect. 2.1, effective cross sections are not strongly coupled to burnup; hence it is sufficient to compute cross sections for the average burnup of a fuel subgroup, provided the range of burnups in the subgroup is not too large (less than 2 GWd/MTU). Nuclide concentrations

Table 2. Set of fuel nuclides used in KENO V.a calculations

$^{234}U^{a}$	$^{83}Kr^{d}$	$^{141}Pr^{b}$
$^{235}U^{a}$	$^{93}Zr^{b}$	$^{143}Nd^{a}$
$^{236}U^{a}$	$^{95}Mo^{a}$	$^{145}Nd^{a}$
$^{238}U^{a}$	$^{99}Tc^{a}$	$^{147}Nd^{c}$
$^{237}Np^{b}$	$^{101}Ru^{b}$	$^{148}Nd^{c}$
$^{238}Pu^{a}$	$^{103}Ru^{c}$	$^{147}Pm^{b}$
$^{239}Pu^{a}$	$^{103}Rh^{a}$	$^{148}Pm^{c}$
$^{240}Pu^{a}$	$^{105}Rh^{c}$	$^{149}Pm^{c}$
$^{241}Pu^{a}$	$^{105}Pd^{b}$	$^{147}Sm^{a}$
$^{242}Pu^{a}$	$^{108}Pd^{b}$	$^{149}Sm^{a}$
$^{241}Am^{a}$	$^{109}Ag^{b}$	$^{150}Sm^{a}$
$^{243}Am^{b}$	$^{135}I^{c}$	$^{151}Sm^{a}$
$^{244}Cm^{b}$	$^{131}Xe^{d}$	$^{152}Sm^{a}$
O^{a}	$^{135}Xe^{c}$	$^{153}Eu^{a}$
	$^{133}Cs^{a}$	$^{154}Eu^{b}$
	$^{134}Cs^{d}$	$^{155}Eu^{b}$
	$^{135}Cs^{a}$	$^{155}Gd^{a}$

[a]The 25 nuclides to be used in burnup credit analysis (ref. 4).
[b]Additional burnup credit nuclides from ref. 1.
[c]Additional reactor physics nuclides from Virginia Power's PDQ calculations (ref. 13).
[d]Additional reactor physics nuclides from Yankee Atomic's CASMO-3/SIMULATE-3 calculations (ref. 14).

for use in the CSASN calculation are provided in SCALE standard composition format in the output of the SNIKR subgroup calculations.

Because fission-product nuclides represent only a small fraction of the total number density of the fuel, fission-product cross sections are relatively insensitive to changes in isotopic content and need only be calculated for one subgroup. This situation is also true of many fuel activation products and minor actinides; however, cross sections for seven actinides are assumed to have a more significant burnup dependence. These isotopes, referred to as the "seven burnup-sensitive actinides," are ^{234}U, ^{235}U, ^{236}U, ^{238}U, ^{239}Pu, ^{240}Pu, and ^{241}Pu. CSASN subgroup fuel pin models include the appropriate SNIKR-computed concentrations for each of these isotopes; the remaining nuclides are included only in the highest burnup subgroup. The highest burnup is chosen because it should result in the lowest resonance absorption, and therefore a higher and more conservative value of k_{eff}; however, the effect is extremely small (<0.1% $\Delta k/k$).

Once cross sections are computed for each fuel subgroup, the SCALE utility module WAX[17] is used to combine all subgroup cross-section working libraries prepared via CSASN into a single working library for subsequent use by KENO V.a. All cross sections from the highest burnup subgroup (containing all fission and activation isotopes) are copied into the combined library. For each of the remaining subgroup cross-section libraries, only the seven burnup-dependent actinides are copied. In addition, for each of the seven burnup-dependent actinides in each subgroup, the cross-section ID number is modified by prefixing the subgroup number to the cross-section ID so that the KENO V.a core model can reference the appropriate cross section for each fuel subgroup. The cross sections with modified ID numbers are then copied into the combined library.

2.5 PREPARATION OF A KENO V.a CORE MODEL

All four reactor models included in this report can be reduced in complexity by taking advantage of the one-eighth core symmetry of assemblies. Thus, it is possible to build a full-core model using a relatively small number of unique assemblies. For each eighth-core assembly location, nuclide concentrations are obtained from assembly-specific SNIKR output in KENO V.a mixing table format; thus there are unique mixture data for each eighth-core assembly location in the model. Within each set of mixing table data, the nuclide ID number of each of the seven burnup-dependent actinides is prefixed by the cross-section set number which represents that assembly (this can be done automatically by SNIKR) so that the effective cross sections computed for the corresponding cross-section set are utilized. These cross sections are located in the working library, prepared as described in the previous subsection.

For each of the reactor models, a single fuel rod was defined for each assembly in the eighth-core representation. This rod definition was used for all fuel locations within the assembly; water-filled guide tubes were placed in the remaining control rod and instrumentation locations. Each assembly was then placed in all symmetric locations in the full-core map; such reactor-specific placement is shown in each of the appropriate volumes. Radially, baffle, core barrel, and thermal shield components were placed outside the core configuration. Axially, top and bottom regions comprised of a uniform mixture of stainless steel and borated water (50/50, by weight) were placed at the top and bottom regions. Vacuum boundary conditions were assumed beyond the reactor vessel model.

Beyond the aspects described above, the geometry of a reactor core model is based on the technical specifications of the specific reactor for which critical calculations are being performed; hence the detailed mechanics of the geometry models are discussed in the subsequent volumes.

The following section (1) discusses the differences between the reactor critical configurations and the results computed for each configuration and (2) provides possible explanations for these differences.

3. SUMMARY OF REACTOR CRITICAL CALCULATIONS

Subsequent volumes of this report describe criticality calculations performed for four reactor configurations: Volume 2 describes criticality calculations for the Tennessee Valley Authority's Sequoyah Unit 2 reactor for Cycle 3; Volume 3 documents the analysis of Virginia Power's Surry Unit 1 reactor for the Cycle 2 core; Volume 4 documents the calculations performed based on GPU Nuclear Corporation's Three Mile Island Unit 1 Cycle 5 core; and, lastly, Volume 5 describes calculations for Virginia Power's North Anna Unit 1 Cycle 5 core. Based on these cores, a total of seven reactor criticals were performed. This section will give an overview of all seven criticals by providing (1) a summary of the key features of each core design and the significant factors at the time of each critical measurement, (2) a description of key differences between the various reactor critical configurations, and (3) the results of criticality calculations for all cases.

3.1 GLOBAL AND BURNUP-DEPENDENT CORE FEATURES

Table 3 lists the seven reactor critical configurations for which criticality calculations have been performed. The "designation" column lists the abbreviations that will be used in this and following sections to distinguish between the different reactor critical measurements. Unless specifically stated otherwise, the names Sequoyah, Surry, TMI, and North Anna refer to the unit and fuel cycle given in the table for each reactor. BOC cases were based on startup measurements performed at the start of the given fuel cycle. The single end-of-cycle (EOC) case is based on normal operating conditions measured at the end of the given fuel cycle. The middle-of-cycle (MOC) case is based on startup measurements performed for Sequoyah after an extended downtime during the fuel cycle. Hot, zero-power (HZP) cases were based on critical conditions established with very low core thermal output (i.e., hot conditions were established using pump heating only). Hot, full-power (HFP) cases were based on full-power operation in an equilibrium state.

Table 4 lists some of the key physical aspects of each of the four core designs. Note that the Surry and TMI assembly designs are very similar in physical dimensions, with the exception that the Surry assembly design contains fewer fuel pins and more guide tubes than the TMI assembly, allowing slightly more moderation in the lattice when all other factors are equal. Furthermore, the TMI core is somewhat larger than the Surry core. The Sequoyah and North Anna assembly lattice designs are significantly different from Surry and TMI; even though they are roughly the same dimensions as those used in the other reactors, the fuel rod pitch and size are somewhat smaller to accommodate the increased number of fuel pins in the assembly. Hence, the neutron energy spectrum within both the Sequoyah and North Anna reactors, while remaining thermal, is likely to be slightly different than the energy spectra of the other reactors. Additionally, the Sequoyah core is larger than both the Surry and TMI cores, while the North Anna core is roughly the same size as the Surry core.

Each of the seven reactor critical scenarios represents a unique set of operating conditions, including factors such as burnup, power, xenon worth, soluble boron concentration, fraction of spent fuel, downtime prior to critical, and temperature conditions. These quantities are summarized in Tables 5 and 6 and demonstrate the range of conditions spanned by these calculations.

Table 3. Summary of reactor critical configurations

Reactor	Cycle No.	Cycle burnup[a]	Power condition[b]	Designation
Sequoyah Unit 2	3	BOC	HZP	Sequoyah BZ
Sequoyah Unit 2	3	BOC	HFP	Sequoyah BF
Sequoyah Unit 2	3	MOC	HFP	Sequoyah MF
Surry Unit 1	2	BOC	HZP	Surry BZ
Surry Unit 1	2	EOC	HFP	Surry EF
Three Mile Island Unit 1	5	BOC	HZP	TMI BZ
North Anna Unit 1	5	BOC	HZP	North Anna BZ

[a]Beginning of cycle (BOC), middle of cycle (MOC), or end of cycle (EOC).
[b] Hot, zero power (HZP) or hot, full power (HFP).

Table 4. Assembly design data

	Sequoyah	Surry	TMI	North Anna
Designer	Westinghouse	Westinghouse	Babcock & Wilcox	Westinghouse
Lattice type	17×17	15×15	15×15	17×17
No. of assemblies	193	157	177	157
No. of fuel rods/assm.	264	204	208	264
No. of guide tubes/assm.	24	20	16	24
No. of instr. tubes/assm.	1	1	1	1
Lattice pitch, cm (in.)	21.504 (8.466)	21.504 (8.466)	21.681 (8.536)	21.504 (8.466)
Rod pitch, cm (in.)	1.25984 (0.496)	1.43002 (0.563)	1.44272 (0.568)	1.25984 (0.496)
Clad OD, cm (in.)	0.94966 (0.374)	1.07188 (0.422)	1.09220 (0.430)	0.94966 (0.374)
Clad ID, cm (in.)	0.83566 (0.329)	0.94844 (0.373)	0.93624 (0.369)	0.83566 (0.329)
Pellet diameter, cm (in.)	0.81915 (0.323)	0.92939 (0.366)	0.93624 (0.369)	0.81915 (0.323)
Approximate fuel volume/assembly(cm^3)	50,900	50,600	52,400	50,900

Table 5. Significant aspects of reactor critical configurations

Reactor critical case	Core-average burnup (MWd/MTU)	Initial enrichment range (wt % ^{235}U)	Burnup range (GWd/MTU)	Soluble boron conc. (ppm)	Fraction of burned fuel in core (%)	Downtime prior to critical (y)
Sequoyah BZ	10,998	2.6 – 3.8	0 – 26.9	1685	64.8	0.42
Sequoyah BF	11,148	2.6 – 3.8	0 – 26.9	1150	64.8	0.42
Sequoyah MF	19,248	2.6 – 3.8	7.3 – 34.6	475	100	2.73
Surry BZ	6,929	1.9 – 3.3	0 – 16.6	1030	46.5	0.27
Surry EF	13,845	1.9 – 3.3	5.1 – 24.1	123	100	0
TMI BZ	11,442	2.6 – 2.9	0 – 28.2	1182	75.8	6.67
North Anna BZ	11,067	3.2 – 3.6	0 – 32.0	1836	56.7	0.37

Table 6. Average temperatures for critical configurations

Reactor critical case	Fuel temperature (K)	Clad temperature (K)	Moderator temperature (K)
Sequoyah BZ	559	559	559
Sequoyah BF	901	628	579
Sequoyah MF	901	628	579
Surry BZ	559	559	559
Surry EF	910	595	569
TMI BZ	551	551	551
North Anna BZ	559	559	559

To validate the analysis methodology used here for general spent fuel applications, it is desirable to perform calculations for configurations that are close to those expected in AFR scenarios. Thus, the burnup, fraction of spent fuel, and downtime were important factors in the selection of these reactor configurations as proposed benchmarks for burnup credit applications. The Sequoyah benchmarks were selected primarily for the MOC core, which at the time of startup had experienced a 2.7-year downtime and consisted of a core completely comprised of burned fuel. The other two Sequoyah configurations were evaluated because the data were readily available as a test of consistency with the MOC case. The TMI benchmark was selected for similar reasons. The core consisted primarily of burned fuel, with all fresh fuel located at the core periphery, where its importance is diminished. Startup occurred after an especially long downtime of 6.6 years. The Surry and North Anna benchmarks, on the other hand, were performed as a comparison with earlier

scoping studies[8] performed for these reactors. The configurations were selected in the earlier analyses primarily because the reactor data and utility-generated isotopic data were readily available at that time, rather than for specific spent fuel characteristics.

In addition to the factors described earlier, reactivity control hardware varied between the four reactor designs. As Westinghouse designs, Sequoyah, Surry, and North Anna utilized similar burnable poison (BP) systems for control of excess reactivity, although the number, placement, and size of BPRs varied between the 15 × 15 and 17 × 17 assembly designs. The specifics of the individual BP systems and their treatment in criticality calculations are addressed in the Sequoyah, Surry, and North Anna volumes (2, 3, and 5, respectively) of this report. The TMI core did not use BPs during cycle 5; however, the core design did include partial length control rods, known as Axial Power Shaping Rods (APSRs), used for axial power shaping. The physical configuration and modeling treatment of the TMI APSR's are discussed in detail in Vol. 4.

3.2 KEY DIFFERENCES BETWEEN REACTOR CRITICAL CONFIGURATIONS

As has been discussed earlier, notable differences exist between the four reactor designs. These differences may introduce biases in criticality calculations due to modeling approximations or assumptions. Insufficient data exist to allow a statistical determination of any trends and biases in the various reactor critical results. However, it is important to recognize those conditions that might result in such differences because these items should be considered in additional reactor critical calculations, as well as in future uncertainty analyses. The remainder of this section discusses possible causes for differences between the reactor criticals.

Some significant differences exist in the physical designs of the reactor cores. The Sequoyah, Surry, and North Anna designs employ BPRs for reactivity control; TMI, on the other hand, utilizes APSRs for axial power shaping. BPRs consist of borosilicate glass run virtually the full length of the active fuel core and are fixed in place; TMI's APSRs, on the other hand, are comprised of a 91.4-cm silver/cadmium/indium plug at the bottom of a water-filled tube, and are moved vertically during operation to optimize power shaping. Boron-based BPRs are primarily thermal absorbers, while Ag-Cd-In rods are strong epithermal absorbers. Additionally, full-length BPR clusters are used in 44 assembly positions in Sequoyah, 28 Surry assemblies, and 68 North Anna assemblies, while partial-length APSR clusters are used only in 8 assemblies in the TMI core. Thus, the three BP-based cores would have a more globally distributed thermal flux depression, as opposed to the TMI core, which would experience more localized epithermal and thermal flux depressions. This difference may indicate that assemblies that contained APSRs in earlier cycles, in which the presence of APSRs was neglected, are not properly modeled in terms of isotopic composition. However, because the position of APSRs changes with time during an operational cycle, it is not possible to model such effects without going into detailed and cumbersome calculations. The end result shows that such effort is not warranted.

Another geometric difference between the reactor designs is the use of a 17 × 17 pin lattice in Sequoyah and North Anna as opposed to a 15 × 15 lattice in the other two core designs. The smaller diameter and pitch used in the 17 × 17 lattice result in a closer approximation to a homogeneous core than that represented by a 15 × 15 lattice, and self-shielding effects are reduced. Hence any bias in the numerical technique used in modeling self-shielding approaches could introduce discrepancies in the results.

The differences in lattice structures may be compounded to some extent by the different amount of ^{235}U enrichment in the different assembly types. Direct comparison of a representative enrichment is difficult: the TMI core was comprised of assemblies with initial enrichments of 2.64 and 2.85 wt %; Sequoyah contained assemblies of five different initial enrichments, ranging from 2.6 to 3.8 wt %; Surry contained four different enrichments, ranging from 1.86 to 3.33 wt %; and North Anna contained essentially three enrichments of 3.21 to 3.60 wt %. Some of these assemblies had burned multiple cycles, some only one cycle, and the remainder contained fresh fuel. However, assuming one can characterize the core enrichment by the average of the initial enrichments of each assembly in the core, then average core enrichments, in wt % ^{235}U, are the following: Sequoyah, 3.4; Surry, 2.6; TMI, 2.8; and North Anna, 3.5. Hence, Sequoyah and North Anna are likely to be more highly enriched cores than either of the other two systems.

Each of the reactor criticals contains some fraction of burned fuel, ranging from about 50% to 100% of all assemblies. Because of the neutron absorption in ^{238}U followed by β decay, ^{239}Pu is present in all burned fuel assemblies; the fractional content will depend on the initial enrichment and assembly burnup. An energy-dependent bias in k_{eff} is known to exist in the 27BURNUPLIB cross-section library for systems containing plutonium.[18,19] This bias is discussed further in the following section. The net effect of this bias will be an increased value of k_{eff} for lower-energy (more thermalized) systems. Note that this plutonium bias is not limited to the 27BURNUPLIB; instead, it appears to be inherent in current plutonium cross-section data.[20,21]

Finally, a source of error that is beyond the domain of the reactor critical models, but may be significant, is due to error in experimental measurements. Startup HZP criticals are generally tightly controlled and are associated with well-characterized measurements. Thus, experimental uncertainties are typically small for such critical cases. HFP conditions obtained at startup are similarly well controlled under startup procedures; however, uncertainties are introduced in temperature distributions across the core, since fuel and clad temperature distributions are not measured directly, and only bulk coolant temperatures are known. [Usually the effect of such uncertainty will be small, because cross sections will change little over the range of nominal temperature uncertainties. In addition, the effect of xenon and temperature feedback mechanisms are not included in the reactor models. This simplification tends to overpredict reactivity in the high-powered (most reactive) assemblies.] EOC conditions, on the other hand, generally are not as well characterized. This situation is the case for the Surry EF case, where soluble boron concentrations were estimated based on operational measurements. In general, spent fuel isotopics are notably different at EOC, because the reactor has operated at full-power equilibrium conditions for a long period prior to the critical configuration. Thus, there are short-lived fission products present that do not appear in configurations that have been subject to downtime prior to startup.

3.3 RESULTS OF CRITICALITY CALCULATIONS

The calculated value of k_{eff} for each of the seven reactor critical configurations is given in Table 7. Also given is the average energy group (AEG) in which fission occurs. The AEG can be used to assess the *relative* energy spectra for each critical configuration, but cannot be converted to determine the average energy for fission, because the relationship between average energy and average energy group is not linear. However, for reference, the energy boundary between groups 19

Table 7. KENO V.a calculated results for reactor critical configurations

Reactor configuration	$k_{eff} \pm \sigma$	Average energy group where fission occurs	Number of histories in Monte Carlo calculation
Sequoyah BZ	1.0039 ± 0.0005	20.487 ± 0.004	1,000,000
Sequoyah BF	1.0067 ± 0.0005	20.382 ± 0.004	1,000,000
Sequoyah MF	1.0046 ± 0.0005	20.444 ± 0.004	1,000,000
Surry BZ	1.0014 ± 0.0005	21.018 ± 0.004	1,000,000
Surry EF	1.0113 ± 0.0005	20.974 ± 0.004	1,000,000
TMI BZ	0.9978 ± 0.0004	20.782 ± 0.003	2,000,000
North Anna BZ	1.0040 ± 0.0005	20.384 ± 0.004	1,000,000

and 20 is 0.8 eV, and the energy boundary between groups 20 and 21 is 0.4 eV. The AEG results indicate that for these particular fuel cycles Surry represents the most thermal system, TMI is intermediate, and Sequoyah and North Anna have the highest average fission energy. Clearly, however, all systems are thermal, and are grouped relatively close together. Note that the four 17 × 17 assembly cores are all grouped together at an average energy corresponding to an AEG of about 20.4, whereas the three 15 × 15 assembly cores are grouped together at an AEG of roughly 20.9, as shown in Fig. 4. Also note that for the Sequoyah and Surry cases, relatively little change is seen in AEG as a function of exposure (BOC, MOC, or EOC).

Values of k_{eff} reported in Table 7 are specified to within 0.01%. Although this indicates greater precision than is reasonable for this type of calculation, the number of significant digits reported is consistent with the number of digits in the uncertainty terms. It was felt to be important to provide the level of uncertainty to demonstrate that the statistical deviation of the calculations had been minimized.

All three Sequoyah criticals are grouped together and appear to be self-consistent, indicating that changes in isotopic concentrations between the three reactor states are reasonably well modeled. Overprediction of k_{eff} may be due to inadequacies in the physical model (including fission products not modeled); however, other influences are possible. Surry BZ is in good agreement with the known critical condition, but like Sequoyah it overpredicts k_{eff} slightly. On the other hand, Surry EF is substantially higher than other cases. This is possibly due to inadequate characterization of EOC conditions, which will be discussed later. The TMI BZ case appears somewhat low relative to the other cases. However, the TMI critical stands out from other cases due to its 6.6-year cooling time prior to restart. Because the fission product ^{155}Eu decays to ^{155}Gd with a 4.7-year half-life, significant amounts of ^{155}Gd are present in the TMI critical relative to other reactor criticals; this isotope is a strong absorber and can significantly affect k_{eff}. Thus, overprediction of ^{155}Eu inventory would result in a reduced calculated value of k_{eff}. Such overprediction is suspected with the use of SCALE 27BURNUPLIB cross sections. [22] Finally, North Anna BZ is very close to Sequoyah BZ, which is very similar in configuration and core conditions (although Sequoyah is a larger core).

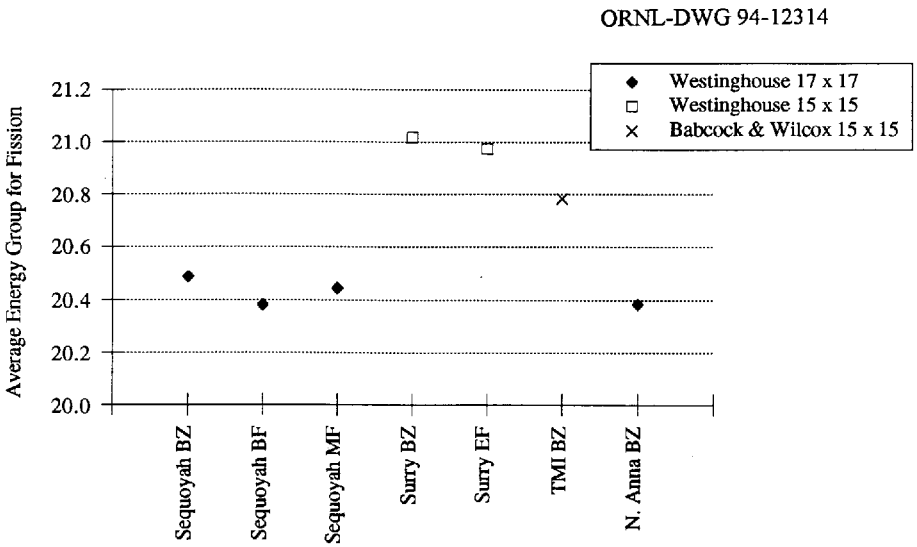

Fig. 4. Average energy group for fission for different assembly designs.

4. CONVERGENCE AND SENSITIVITY TESTING

Beyond the calculations discussed in the previous section, additional calculations were performed in order to verify that the results obtained were adequately modeled and completely converged. The stochastic nature of the Monte Carlo methods in KENO V.a can be biased by various parameter specifications. For the reactor criticals, the two parameters that were felt to have the most potential for bias or error in the calculated value of k_{eff} were the number of particle histories tracked and the neutron starting distribution. Additionally, the assumed order of scattering and the number of isotopes used were investigated to assess the sensitivity of the models to these parameters. The remainder of this section describes the findings of these studies.

The number of neutron histories considered is a key factor in the accuracy of any Monte Carlo simulation; an insufficient number of histories will result in an inadequate statistical basis for the prediction of k_{eff}. However, because of the complexity and size of the reactor critical models described in this report, a statistically converged solution may not necessarily be representative of the reactor k_{eff}. Even when sufficient histories have been completed to obtain an acceptably small statistical deviation, one must verify that all important regions of the reactor have been adequately sampled. Because of the random nature of the Monte Carlo technique, it is possible for a majority of sampling to occur in a subregion of the core; if this subregion is not representative of the core-wide behavior, an erroneous k_{eff} will be reported, heavily weighted by the k_{eff} of the dominant subregion. One approach to test for statistically uniform sampling is to rerun the same calculations using different starting (seed) random numbers. Valid starting numbers may be obtained from KENO V.a by selecting the "final" random number printed in the output of the previous calculation.

For each of the seven reactor criticals, calculations were repeated using valid starting seeds. Results of these calculations are given in Table 8. All calculations were repeated at least once; both Surry EF and TMI BZ were recalculated three times since the results of these cases seem the most inconsistent relative to the other five critical calculations. The Δk column of Table 9 shows the difference between the nominal value of k_{eff} computed here relative to the result reported in Table 7. Thus, these calculations were found to be consistent with the results of the original base cases within statistical uncertainty bounds. Hence, all values of k_{eff} are considered to be spatially converged.

The second issue, the neutron starting distribution, also relates to the size of the reactor models. The neutron starting distribution represents the initial guess of the spatial distribution of fission density when starting a generation of neutrons. Although the burnup-dependent isotopic concentrations were assumed uniform along the length of the fuel, the shape of the fission distribution driven by fresh fuel will be nonuniform and will be roughly the shape of a cosine (albeit somewhat flattened). The default starting distribution, used in all of the reactor critical calculations, is a spatially uniform distribution in all fissile material. If the starting distribution is a poor approximation to reality and insufficient generations are used, the solution will be biased by the starting distribution. Because of the length of the fuel rods (~366 cm) and the fact that the end regions of a fuel rod may contribute relatively little to the total number of fissions occurring in the rod, it was considered possible that the rod ends were inappropriately weighted when using the default starting profile. To test the effect of the starting distribution on the reactor critical solutions, all cases were rerun with two distinctly different initial starting distributions: an axial cosine shape and a uniform distribution located only in the bottom 10 cm of the fuel. Results of these calculations are given in Table 9. As in Table 8,

Table 8. KENO V.a calculated results for different starting seed numbers

Reactor configuration	Starting random No. (hexadecimal)	Number of neutron histories	$k_{eff} \pm \sigma$	Δk
Sequoyah BZ	3EEC20590968	1,000,000	1.0033 ± 0.0005	-0.0006
Sequoyah BF	3EEC20590968	1,000,000	1.0065 ± 0.0005	-0.0002
Sequoyah MF	3EEC20590968	1,000,000	1.0049 ± 0.0005	0.0003
Surry BZ	3EEC20590968	1,000,000	1.0007 ± 0.0005	-0.0007
Surry EF	3EEC20590968	1,000,000	1.0103 ± 0.0005	-0.0010
Surry EF	0CB4296901B2	400,000	1.0100 ± 0.0008	-0.0013
Surry EF	515812762B9D	400,000	1.0118 ± 0.0008	0.0005
TMI BZ	3EEC20590968	1,000,000	0.9968 ± 0.0005	-0.0010
TMI BZ	698D7B591F37	400,000	0.9972 ± 0.0007	-0.0006
TMI BZ	4BCE5AE20D21	400,000	0.9990 ± 0.0007	0.0012
North Anna BZ	3EEC20590968	1,000,000	1.0026 ± 0.0005	-0.0014

Table 9. KENO V.a calculated results for different starting distributions

Reactor configuration	Starting distribution	Number of neutron histories	$k_{eff} \pm \sigma$	Δk
Sequoyah BZ	Cosine	1,000,000	1.0049 ± 0.0005	0.0010
Sequoyah BZ	Uniform - bottom 10 cm	1,000,000	1.0026 ± 0.0005	-0.0013
Sequoyah BF	Cosine	1,000,000	1.0062 ± 0.0005	-0.0005
Sequoyah BF	Uniform - bottom 10 cm	1,000,000	1.0050 ± 0.0006	-0.0017
Sequoyah MF	Cosine	1,000,000	1.0053 ± 0.0005	0.0007
Sequoyah MF	Uniform - bottom 10 cm	1,000,000	1.0035 ± 0.0007	0.0011
Surry BZ	Cosine	1,000,000	1.0010 ± 0.0005	-0.0004
Surry BZ	Uniform - bottom 10 cm	1,000,000	1.0003 ± 0.0005	-0.0011
Surry EF	Cosine	1,000,000	1.0110 ± 0.0005	-0.0003
Surry EF	Uniform - bottom 10 cm	1,000,000	1.0108 ± 0.0005	-0.0005
TMI BZ	Cosine	1,000,000	0.9983 ± 0.0005	0.0005
TMI BZ	Uniform - bottom 10 cm	1,000,000	0.9971 ± 0.0007	-0.0007
North Anna BZ	Cosine	1,000,000	1.0029 ± 0.0005	-0.0011
North Anna BZ	Uniform - bottom 10 cm	1,000,000	1.0047 ± 0.0005	0.0007

the Δk column shows the difference between the nominal value of k_{eff} computed here relative to the result reported in Table 7. Again, all results were found to be consistent with the results of the original base cases within statistical uncertainties. This implies the solution is insensitive to the starting distribution.

Some of the critical calculations in this study were originally run based on default second-order (P_1) scattering cross sections. This approximation was considered sufficient for reactor calculations because fluxes should remain isotropic through most of the core, except near the periphery, which contributes little to the net value of k_{eff}. To test this hypothesis, and to verify that no numerically induced bias resulted from the use of higher order scattering, calculations were rerun using fourth-order (P_3) scattering cross sections. No significant change in k_{eff} was noted as a result of this change. All results reported in Table 7 were based on fourth-order scattering.

Finally, a study was performed to assess the relative worth of the nuclides included and neglected in the reactor critical models. As discussed earlier, 48 nuclides were included in all reactor critical calculations. These nuclides are listed in Table 2 and are believed to be the 48 most important nuclides for spent fuel criticality calculations in terms of their effect on k_{eff}. Calculations were repeated using (1) the 25 nuclides recommended for burnup credit applications[4] (listed in Table 2 with footnote label "a"), and (2) all 193 nuclides available in the SCALE 27-group burnup library. The 193-nuclide calculation was performed for the Surry and TMI configurations only; no additional calculations were performed for the Sequoyah BZ case. The values of k_{eff} calculated using each of these sets of nuclides are given in Tables 10 and 11. The Δk columns give the change in the nominal value of k_{eff} relative to the 48-nuclide-based results.

These results verify that there is conservatism in the use of the 25 BUC nuclides for design calculations related to burnup credit. For reactor criticals the conservatism ranges from roughly 1% Δk at HZP conditions to 4 to 5% Δk for HFP. The difference between the two states results from the fact that ^{135}Xe is not included among the burnup credit nuclides because it decays rapidly after shutdown; Table 12 shows that the ^{135}Xe worth under HFP conditions is in the 2.5 to 3% Δk range. ^{135}Xe burns in rapidly under full-power conditions, but does not accumulate under HZP startup conditions.

Based on the Surry and TMI 193-nuclide calculations (with 145 additional nuclides), results indicate that the 48 nuclides included in the reactor critical calculations adequately represent the worth of all nuclides present (i.e., the worth of the remaining nuclides is small). For Surry EF and TMI BZ, the worth of the additional 145 nuclides is less than 0.5%. The 1.1% Δk worth of the additional 145 isotopes for the Surry BZ case is likely to result from short-lived decay products not included in the 48-isotope set; such nuclides would have been burned out in the Surry EF case, and would have decayed away prior to the TMI BZ startup. Table 12 also shows the estimated worth of the burnup credit fission products (fission-product subset of the 25 burnup credit nuclides listed in Table 2) plus ^{241}Am and the estimated worth of the remaining fission products plus all other nonuranium, nonplutonium actinides. These values were obtained by recalculation of k_{eff} after removing each of the above sets of isotopes from each critical configuration. The worth of ^{135}Xe was not included in the worth of the full set of fission products, since it is only present under HFP conditions. These results demonstrate that even in reactor critical configurations most of the fission-product worth is represented by the 25 burnup credit nuclides (listed in Table 2).

Table 10. k_{eff} based on 25-nuclide model

Reactor configuration	$k_{eff} \pm \sigma$ 25-Nuclide model	$k_{eff} \pm \sigma$ 48-Nuclide model (from Table 7)	Δk ($k_{eff, 25} - k_{eff, 48}$)
Sequoyah BF	1.0461 ± 0.0005	1.0067 ± 0.0005	0.0394
Sequoyah MF	1.0530 ± 0.0005	1.0046 ± 0.0005	0.0484
Surry BZ	1.0096 ± 0.0005	1.0014 ± 0.0005	0.0082
Surry EF	1.0619 ± 0.0005	1.0113 ± 0.0005	0.0506
TMI BZ	1.0093 ± 0.0004	0.9978 ± 0.0004	0.0115
North Anna BZ	1.0104 ± 0.0005	1.0040 ± 0.0005	0.0064

Table 11. k_{eff} based on 193-nuclide model

Reactor configuration	$k_{eff} \pm \sigma$ 193-nuclide model	$k_{eff} \pm \sigma$ 48-nuclide model (from Table 7)	Δk ($k_{eff, 193} - k_{eff, 48}$)
Surry BZ	0.9900 ± 0.0005	1.0014 ± 0.0005	-0.0114
Surry EF	1.0072 ± 0.0005	1.0113 ± 0.0005	-0.0041
TMI BZ	0.9944 ± 0.0003	0.9978 ± 0.0004	-0.0034
North Anna BZ	1.0027 ± 0.0005	1.0040 ± 0.0005	-0.0013

Table 12. Incremental worth of fission products and parasitic absorbers in reactor criticals

Configuration	Δk, ^{135}Xe (%)	Δk, BUC fission products + ^{241}Am[a] (%)	Δk, Additional fission products + nonproductive actinides (%)[a]
Sequoyah BZ	0	-3.45	-0.71
Sequoyah BF	-2.66	-3.28	-1.46[b]
Sequoyah MF	-2.96	-6.81	-2.05[b]
Surry BZ	0	-2.70	-0.93
Surry EF	-2.85	-4.99	-2.77[b]
TMI BZ	0	-4.90	-1.01
North Anna BZ	0	-2.42	-0.63

[a]Isotopes are specified in Table 2.
[b]Xenon resulting from HFP operation was omitted.

5. COMPARISON WITH CALCULATIONS OF LWR-TYPE CRITICAL EXPERIMENTS

Calculations have been performed based on LWR-type fuel experimental measurements using the same 27BURNUPLIB cross-section library used in the reactor critical calculations.[19] These experiments, used as the basis for cross-section validation studies, were selected as representative of "typical" low-enrichment UO_2 LWR assemblies. The selections contain enrichments ranging from 2.35 to 5.74 wt % ^{235}U. Cadmium, boron, boral, boroflex, Ag-In-Cd, gadolinium, polyethylene, and stainless steel were used as absorbers in various experiments, and uranium, lead, and steel reflectors were included. Various lattice shapes and pitches were used, with moderator-to-fuel volume ratios of 0.509 to 5.067. Both UO_2 and mixed-oxide (MOX) fuels were used. Results are summarized in Figs. 5 and 6. Figure 5 shows the values of k_{eff} as a function of the AEG, based on the 27-group energy structure plotted with the results of experiment-based MOX calculations. The solid line is a linear fit to the experiment-based results and shows a positive bias in k_{eff} with AEG. [Due to the somewhat limited amount of data available, the slope of the line should not be taken to represent the magnitude of the bias; instead, it simply indicates the trend for k_{eff} to increase with increasing AEG (i.e., more thermalized, or lower energy, systems).] Figure 6 shows the same information for reactor critical results plotted with the results of critical experiment-based UO_2 calculations. Note that the results of the reactor critical calculations in this study are more consistent with the trend of the results of the MOX criticals; this behavior is expected. The isotopic content of the MOX criticals, although not prototypic, more closely resembles the plutonium-bearing spent fuel assemblies of the reactor criticals than do the fresh fuel UO_2 criticals.

Based on the comparison to MOX criticals shown in Fig. 5, it would appear that Surry BZ and TMI BZ are most consistent with the experimental measurements, and that only the Surry EF case would be considered as an outlying result. Sequoyah results are self-consistent and are relatively close to the results of the experimental cases, as is the North Anna result. Note that the Surry BZ case is closest to the fit to the zero-power MOX criticals, and that all full-power cases (Sequoyah BF, Sequoyah MF, and Surry EF) are more removed from the data. This trend indicates that perhaps aspects of full-power operation (e.g., nuclides present, temperature effects, axial power distributions, xenon distributions, etc.) are not being well represented in the KENO V.a models.

The error bars shown in Figs. 5 and 6 indicate the statistical uncertainty of the value of k_{eff} based on the number of histories run. Uncertainties in the calculated value of the AEG are also present, but these uncertainties are significantly smaller and are much less than the size of the plotting symbols used in the figure. The plotted uncertainties do not include assessment of other modelling uncertainties or biases, so that the total uncertainty associated with any point in the figure is doubtless larger than that shown in the figure. The treatment of such uncertainties is discussed further in the concluding section of this volume.

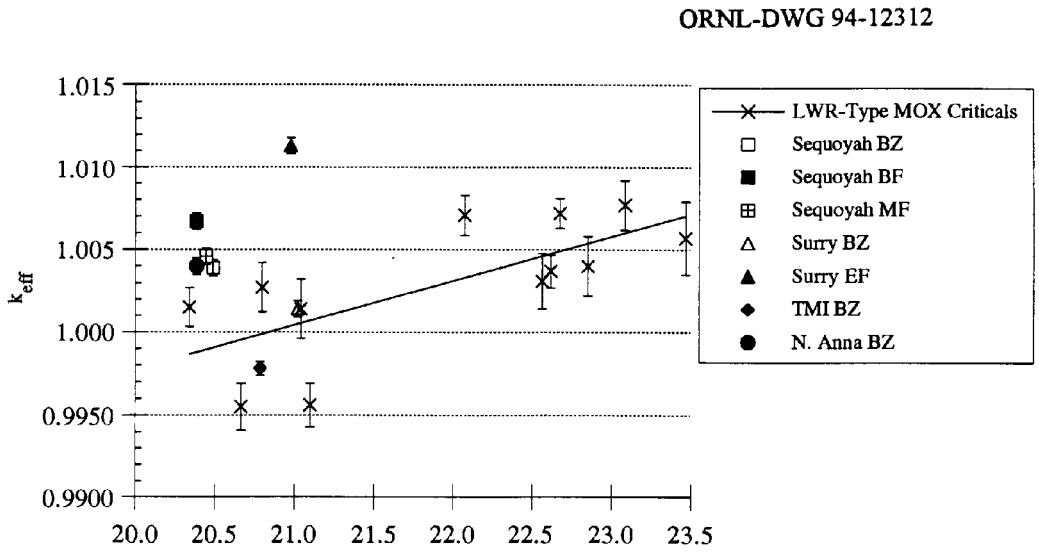

Fig. 5. Comparison of results from reactor criticals to results from MOX LWR-type fuel critical experiments.

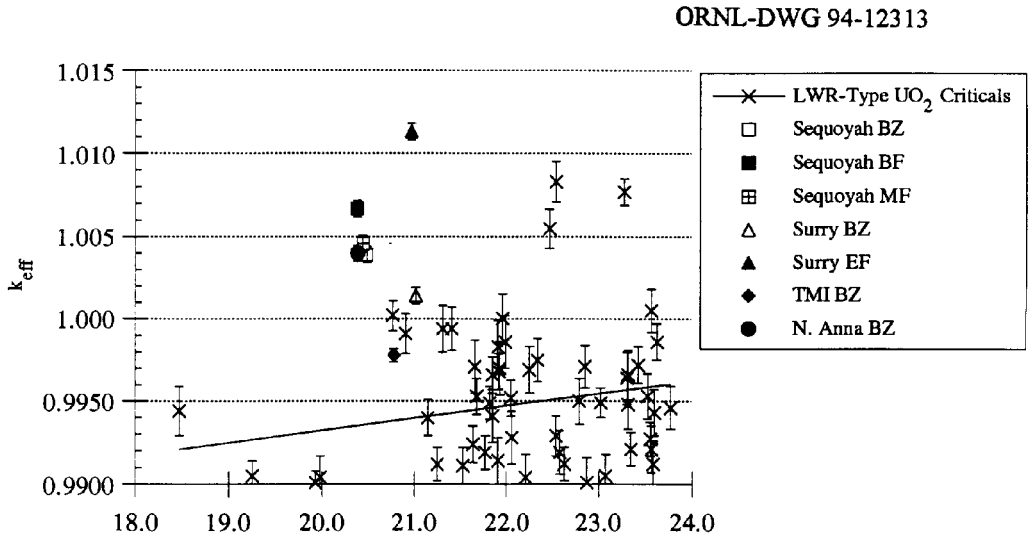

Fig. 6. Comparison of results from reactor criticals to results from fresh fuel (UO_2) LWR-type fuel critical experiments.

6. COMPARISON WITH EARLIER REACTOR CRITICAL CALCULATIONS

The methodology described in this document has been developed to provide a straightforward, easily reproduced approach requiring only the basic assembly data that would typically be available to a cask designer for use in the design of a burnup credit cask. However, as mentioned earlier, preliminary scoping calculations were performed in an initial investigative study to determine the key aspects of isotopic calculations in reactor environments.[8] Because the results of the earlier work have been previously published, it was felt necessary to include a comparison of the earlier results to those obtained using this approach, and to discuss the differences between the two sets of results.

The earlier analysis method involved a complex isotopic calculational procedure in an attempt to match the isotopic results obtained using detailed 3-D reactor physics calculations performed by Virginia Power for the Surry Unit 1 Cycle 2 core. Results from these calculations are reported in ref. 8 and are summarized in Tables 13 and 14. Each of the KENO V.a calculations was based on 500 neutrons per generation and a total of 60,000 neutron histories. Table 13 shows the difference between the nominal value of k_{eff} computed in the preliminary study and the current results using the recommended methods reported here. However, the earlier methodology used all 193 nuclides in the 27BURNUPLIB cross-section library. Thus, Table 14 shows the difference between the scoping result and that obtained using the revised methodology keeping all 193 nuclides (as given in Table 11).

Relative to the reactor critical results presented based on the current methodology, the scoping results are from 1.5 to 2.5% low for SAS2H/ORIGEN-S isotopics based on 48 nuclides, but are on the order of 1.0 to 1.5% low compared with 193 nuclide isotopics. These differences are felt to be caused by several factors, including fewer fuel groups; fewer neutrons per generation and fewer histories; and the use of a complex interface program to prepare the nuclear data. However, these results show the same trends observed for the reactor critical results of Table 7 (i.e., Surry EF results are higher than those obtained for the other configurations).

It is important to emphasize that the earlier work was investigative in nature and performed to help develop the approach used in the current methodology. Because of the complexity of the earlier work, the results reported for that study are not easily reproducible, and therefore have not been investigated further to determine the exact areas of deficiency.

Table 13. Results of earlier methodology compared to current 48-nuclide results

Reactor configuration	$k_{eff} \pm \sigma$ earlier model	$k_{eff} \pm \sigma$ current 48-nuclide model	Δk_{48} ($k_{eff,\ earlier} - k_{eff,\ 48}$)
Surry BZ	0.9757 ± 0.0022	1.0014 ± 0.0005	-0.0257
Surry EF	0.9960 ± 0.0035	1.0113 ± 0.0005	-0.0153

Table 14. Results of earlier methodology compared to current 193-nuclide results

Reactor configuration	$k_{eff} \pm \sigma$ earlier model	$k_{eff} \pm \sigma$ current 193-nuclide model	Δk_{193} ($k_{eff,\ earlier} - k_{eff,\ 193}$)
Surry BZ	0.9757 ± 0.0022	0.9900 ± 0.0005	-0.0143
Surry EF	0.9960 ± 0.0035	1.0072 ± 0.0005	-0.0112

7. CONCLUSIONS

This volume (1) provides an overview of the methodology applied in the criticality calculations performed based on reactor critical data, (2) summarizes and compares the differences between reactor configurations and the results of the critical calculations for these configurations, (3) discusses sensitivity and convergence testing, and (4) compares reactor critical results to those obtained for results obtained for similar composition LWR-type critical experiments. Clearly, as evidenced by the results presented in Table 7, the seven reactor critical calculations demonstrate the ability to predict a k_{eff} very close to the known value of 1.0, based on relatively little detail of the core operation. Such limited information is expected to be the class of data available when performing burnup credit calculations in cask design. Thus, the methodology described herein is appropriate for use in burnup credit analyses related to spent fuel applications. However, in applying this methodology, one must be aware of uncertainties and biases present in such an analysis and the limitations of the methodology relative to these sources of error.

It is neither desired nor desirable to base spent fuel calculations on the unique operating history of each fuel pin in each assembly in a core. Hence, it is necessary to make assumptions as to what approximations are suitable in representing the composition of a spent fuel assembly from a reactor core. The methodology described in Sect. 2 of this report provides a procedure for approximating the composition of a core; additional details related to the specific designs included in this report are given in Sect. 2 of each of the reactor-specific volumes, Vols. 2 through 5. The assumptions inherent in these procedures include the following: resonance processing of cross sections to account for lattice effects (heterogeneity) is relatively insensitive over small burnup ranges (<2 GWd/MTU), variations in isotopic concentrations within an assembly are not significant and can be represented by concentrations based on assembly-averaged burnup; isotopic concentrations for a given burnup can be approximated by interpolation between fixed burnup steps; one can neglect the effect of absorbing materials (i.e., CRs or BPRs) in a given assembly for cycles prior to the cycle in which critical conditions are measured; and axial temperature distributions in moderator are adequately represented by an average bulk coolant temperature for HFP conditions. Results indicate that the combined effect of these assumptions is conservative. All but the TMI BZ calculation give values of k_{eff} greater than unity; the TMI BZ result is less than 1.0, perhaps due to overestimation of ^{155}Gd inventories after the 6.6-year cooling time. Furthermore, recent validation work for LWR-type critical experiments[21] indicates that the use of more recent ENDF/B-V cross sections in a 44-group library developed for LWR applications will result in an increase in the value of k_{eff} by roughly 0.005.

Based on the data presented here and in the subsequent volumes of this report, the methodology employed in the generation of spent fuel isotopics and the criticality calculations using those isotopes is valid for burnup credit analyses. Further validation of the SCALE SAS2H sequence for generating spent fuel isotopics has been performed by comparison of calculated results with measured spent fuel chemical assay data.[22] The criticality methods of CSAS/KENO V.a are validated against LWR-type fresh fuel critical experiments (both UO_2 and MOX) in ref. 19.

REFERENCES

1. T. L. Sanders and R. M. Westfall, "Feasibility and Incentives for Burnup Credit in Spent Fuel Transport Casks," *Nucl. Sci. Eng.* 1041 (1990).

2. *American National Standard for Nuclear Criticality Safety in Operations with Fissionable Materials Outside Reactors*, ANSI/ANS-8.1-1983.

3. *SCALE: A Modular Code System for Performing Standardized Computer Analyses for Licensing Evaluation*, NUREG/CR-0200, Rev. 4 (ORNL/NUREG/CSD-2/R4), Vols. I, II, and III (draft February 1990). Available from Radiation Shielding Information Center as CCC-545.

4. M. C. Brady and T. L. Sanders, "A Validated Methodology for Evaluating Burnup Credit in Spent Fuel Casks," *Proceedings of International Conference on Nuclear Criticality Safety*, Christ Church, Oxford, United Kingdom, September 9-13, 1991.

5. O. W. Hermann and C. V. Parks, "SAS2H: A Coupled One-Dimensional Depletion and Shielding Analysis Code," Sect. S2 of *SCALE: A Modular Code System for Performing Standardized Computer Analyses for Licensing Evaluation*, NUREG/CR-0200, Rev. 4 (ORNL/NUREG/CSD-2/R4), Vols. I, II, and III (draft February 1990). Available from Radiation Shielding Information Center as CCC-545.

6. N. F. Landers and L. M. Petrie, "CSAS4: An Enhanced Criticality Safety Analysis Module with an Optimum Pitch Search," Sect. C4 of *SCALE: A Modular Code System for Performing Standardized Computer Analyses for Licensing Evaluation*, NUREG/CR-0200, Rev. 4 (ORNL/NUREG/CSD-2/R4), Vols. I, II, and III (draft February 1990). Available from Radiation Shielding Information Center as CCC-545.

7. L. M. Petrie and N. F. Landers, "KENO V.a: An Improved Monte Carlo Criticality Program with Supergrouping," Sect. F11 of *SCALE: A Modular Code System for Performing Standardized Computer Analyses for Licensing Evaluation*, NUREG/CR-0200, Rev. 4 (ORNL/NUREG/CSD-2/R4), Vols. I, II, and III (draft February 1990). Available from Radiation Shielding Information Center as CCC-545.

8. J.-P. Renier and C. V. Parks, "Reactor Critical Calculatons for Validation of Burnup Credit Analysis Methods," *Trans. Am. Nucl. Soc.* **62**, 308 (1990).

9. O. W. Hermann and R. M. Westfall, "ORIGEN-S: A SCALE System Module to Calculate Fuel-Depletion, Actinide Transmutation, Fission Product Buildup and Decay, and Associated Radiation Source Terms," Sect. F7 of *SCALE: A Modular Code System for Performing Standardized Computer Analyses for Licensing Evaluation*, NUREG/CR-0200, Rev. 5 (ORNL/NUREG/CSD-2/R5), Vols. 1, 2 and 3 (draft November 1993). Available from Radiation Shielding Information Center as CCC-545.

10. N. M. Greene, "BONAMI-S: Resonance Self-Shielding by the Bondarenko Method," Sect. F1 of *SCALE: A Modular Code System for Performing Standardized Computer Analyses for Licensing Evaluation*, NUREG/CR-0200, Rev. 4 (ORNL/NUREG/CSD-2/R4), Vols. I, II, and III (draft February 1990). Available from Radiation Shielding Information Center as CCC-545.

11. N. M. Greene, L. M. Petrie, and R. M. Westfall, "NITAWL-II: SCALE System Module for Performing Resonance Shielding and Working Library Production," Sect. F2 of *SCALE: A Modular Code System for Performing Standardized Computer Analyses for Licensing Evaluation*, NUREG/CR-0200, Rev. 4 (ORNL/NUREG/CSD-2/R4), Vols. I, II, and III (draft February 1990). Available from Radiation Shielding Information Center as CCC-545.

12. B. L. Broadhead et al., *Investigation of Nuclide Importance to Functional Requirements Related to Transport and Long-Term Storage of LWR Spent Fuel*, ORNL/TM-12742, Martin Marietta Energy Systems, Inc., Oak Ridge Natl. Lab. (in press).

13. B. H. Wakeman and S. A. Ahmed, *Evaluation of Burnup Credit for Dry Storage Casks*, EPRI-NP-6494, Electric Power Research Institute, August 1989.

14. D. G. Napolitano and D. G. Adli, "Burnup Credit Criticality Analysis Using Advanced Nodal Techniques," Yankee Atomic Electric Co., March 1992.

15. O. W. Hermann and R. M. Westfall, "ORIGEN-S: SCALE System Module to Calculate Fuel Depletion, Actinide Transmutation, Fission Product Buildup and Decay, and Associated Radiation Source Terms," Sect. F7 of *SCALE: A Modular Code System for Performing Standardized Computer Analyses for Licensing Evaluation*, NUREG/CR-0200, Rev. 4 (ORNL/NUREG/CSD-2/R4), Vols. I, II, and III (draft November 1993). Available from Radiation Shielding Information Center as CCC-545.

16. M. C. Brady et al., "Comparison of Analysis Methods for Burnup Credit Applications," pp. 771-778 in *Proc. of 9th International Symposium on the Packaging and Transportation of Radioactive Materials*, June 11-15, 1989, Washington, D.C., CONF-890631, Vol. 2, 1989.

17. N. M. Greene, "User's Guide for Utility Modules," Sect. M15 of *SCALE: A Modular Code System for Performing Standardized Computer Analyses for Licensing Evaluation*, NUREG/CR-0200, Rev. 4 (ORNL/NUREG/CSD-2/R4), Vols. I, II, and III (draft February 1990). Available from Radiation Shielding Information Center as CCC-545.

18. R. T. Primm, III, *Validation Studies for KENO IV with Mixed Plutonium-Uranium Critical Experiments*, ORNL/TM-9668, November 1985.

19. S. M. Bowman and M. D. DeHart, "Validation of SCALE-4 for Burnup Credit Applications," Accepted for publication in *Nuclear Technology*.

20. R. J. Brissenden, "Increasing the Physical Realism of the MONK Criticality Code," *Proc. of the Topical Meeting on Physics and Methods in Criticality Safety*, Sept. 19-23, 1993, Nashville, TN, pp. 51-57.

21. M. D. DeHart and S. M. Bowman, *Validation of the SCALE Broad Structure 44-Group ENDF/B-V Cross-Section Library for Use in Criticality Safety Analyses*, NUREG/CR-6102 (ORNL/TM-12460), 1994.

22. O. W. Hermann et al., *Validation of the SCALE System For PWR Spent Fuel Isotopic Composition Analyses*, ORNL/TM-12667 (in press).

INTERNAL DISTRIBUTION

1. C. W. Alexander
2-3. S. M. Bowman
4. B. L. Broadhead
5. J. A. Bucholz
6. R. D. Dabbs
7-8. M. D. DeHart
9. M. B. Emmett
10. N. M. Greene
11. O. W. Hermann
12. M. Kuliasha
13. L. C. Leal
14. S. B. Ludwig
15. S. K. Martin
16. G. E. Michaels
17. B. D. Murphy
18-22. L. F. Norris
23. J. V. Pace
24-28. C. V. Parks
29. L. M. Petrie
30. R. T. Primm
31. J.-P. Renier
32. J. W. Roddy
33. R. W. Roussin
34. J. C. Ryman
35. C. H. Shappert
36. R. M. Westfall
37. B. A. Worley
38. R. Q. Wright
39-40. Laboratory Records Dept.
41. Laboratory Records, ORNL-RC Document Reference Section
42. ORNL Y-12 Research Library
43. Central Research Library
44. ORNL Patent Section

EXTERNAL DISTRIBUTION

45. R. Anderson, General Nuclear Systems, Inc., 220 Stoneridge Dr., Columbia, SC 29210
46. M. G. Bailey, Office of Nuclear Material Safety & Safeguards, U.S. Nuclear Regulatory Commission, MS TWFN 8F5, Washington, DC 20555
47. L. Barrett, Office of Civilian Radioactive Waste Management, RW-232 20545, U.S. Department of Energy, Washington, DC 20545
48. P. Baylor, Office of Civilian Radioactive Waste Management, RW-36, U.S. Department of Energy, Washington, DC 20545
49. C. J. Benson, Bettis Atomic Power Laboratory, P.O. Box 79, West Mifflin, PA 15122
50. J. Bickel, U.S. Department of Energy, Albuquerque Operations Office, P.O. Box 5400, Albuquerque, NM 87115
51. L. Blalock, U.S. Department of Energy, M-261 Quince Orchard, Washington, DC 20585-0002
52. J. Boshoven, GA Technologies, Inc., P.O. Box 85608, 10955 John J. Hopkins Dr., San Diego, CA 92121
53. M. C. Brady, Sandia National Laboratories, 101 Convention Center Drive, Suite 880, Las Vegas, NV 89109
54. P. Bunton, U.S. Department of Energy, RW-1, Washington, DC 20545
55. R. J. Cacciapouti, Yankee Atomic Electric Co., 1617 Worcester Rd., Framington, MA 01701
56. R. Carlson, Lawrence Livermore National Laboratory, P.O. Box 808, Livermore, CA 94550
57. C. R. Chappell, U.S. Nuclear Regulatory Commission, Office of Nuclear Materials Safety and Safeguards, TWFN 8F5, Washington, DC 20555
58. J. S. Choi, Lawrence Livermore National Laboratory, P.O. Box 808, Livermore, CA 94550
59. J. Clark, 2650 Park Tower Drive, Suite 800, Vienna, VA 22180

60. J. Conde, Consejo de Seguridad Nuclear, Justo Dorado, 11, 28040 Madrid, Spain
61. D. R. Conners, Bettis Atomic Power Laboratory, P.O. Box 79, West Mifflin, PA 15122
62. M. Conroy, U.S. Department of Energy, M-261 Quince Orchard, Washington, DC 20585-0002
63. P. J. Cooper, Sandia National Laboratories, P.O. Box 5800, Albuquerque, NM 87185-0716
64. W. Davidson, Los Alamos National Laboratory, Group A4, MSF-611, Los Alamos, NM 87845
65-67. F. J. Davis, Sandia National Laboratories, P.O. Box 5800, Div. 6302, MS 1333, Albuquerque, NM 87185-0716
68. D. Dawson, Transnuclear, Inc., 2 Skyline Dr., Hawthorne, NY 10532-2120
69. T. W. Doering, TESS, B&W Fuel Co., MS 423, Suite 527, P.O. Box 98608, 101 Convention Center Drive, Las Vegas, NV 89109
70. R. Doman, Nuclear Packaging, Inc., 1010 S. 336th St., Suite 220, Federal Way, WA 98003
71. E. Easton, U.S. Nuclear Regulatory Commission, Office of Nuclear Materials Safety and Safeguards, Washington, DC 20555
72. R. C. Ewing, Sandia National Laboratories, P.O. Box 5800, Div. 6643, MS 0716, Albuquerque, NM 87185-0716
73. C. Garcia, U.S. Department of Energy, Albuquerque Operations Office, P.O. Box 5400, Albuquerque, NM 87115
74. S. Hanauer, U.S. Department of Energy, RW-22, Washington, DC 20545
75. C. Haughney, U.S. Nuclear Regulatory Commission, Office of Nuclear Materials Safety and Safeguards, TWFN 8F5, Washington, DC 20555
76. L. Hassler, Babcock & Wilcox, P.O. Box 10935, Lynchburg, VA 24506-0935
77. E. Johnson, E. R. Johnson Associates, Inc., 9302 Lee Hwy, Suite 200, Fairfax, VA 22031
78. R. Kelleher, International Atomic Energy Agency, Division of Publications, Wagramerstrasse 5, P.O. Box 100, Vienna, Austria A-1400
79. R. Kidman, Los Alamos National Laboratory, Group A4, MSF-611, Los Alamos, NM 87845
80. C. Kouts, Office of Civilian Radioactive Waste Management, RW-36, U.S. Department of Energy, Washington, DC 20545
81. S. Kraft, Nuclear Energy Institute, 1776 I Street, Suite 400, Washington, DC 20086
82. P. Krishna, TRW Environmental Safety Systems, 600 Maryland Ave. S.W., Suite 695, Washington, DC 20024
83. A. Kubo, 2650 Park Tower Drive, Suite 800, Vienna, VA 22180
84. W. H. Lake, Office of Civilian Radioactive Waste Management, U.S. Department of Energy, RW-46, Washington, DC 20585
85-87. R. Lambert, Electric Power Research Institute, 3412 Hillview Ave., Palo Alto, CA 94304
88-90. D. Lancaster, 2650 Park Tower Drive, Suite 800, Vienna, VA 22180
91. D. Langstaff, U.S. Department of Energy, Richland Operations Office, P.O. Box 550, Richland, WA 99352
92. D. Lillian, U.S. Department of Energy, M-261 Quince Orchard, Washington, DC 20585-0002
93. C. Marotta, 1504 Columbia Ave., Rockville, MD 20850
94. M. Mason, Transnuclear, Two Skyline Drive, Hawthorne, NY 10532-2120
95. J. Massey, Sierra Nuclear Corporation, 5619 Scotts Valley Drive, Number 240, Scotts Valley, CA 95066
96. W. Mings, U.S. Department of Energy, Idaho Operations Office, 550 2nd St., Idaho Falls, ID 83401
97. A. Mobashevan, Roy F. Weston, Inc., 955 L'Enfant Plaza, SW, 8th Floor, Washington, DC 20024
98. R. Morgan, 2650 Park Tower Drive, Suite 800, Vienna, VA 22180
99. P. K. Nair, Manager, Engineered Barrier System, Center for Nuclear Waste Regulatory Analyses, Southwest Research Institute, 6220 Culebra Road, San Antonio, TX 78238-5166
100. D. Napolitano, Nuclear Assurance Corp., 5720 Peachtree Parkway, Norcross, GA 30092

101. C. W. Nilsen, Office of Nuclear Material Safety and Safeguards, U.S. Nuclear Regulatory Commission, MS TWFN-9F29, Washington, DC 20555
102. D. J. Nolan, 2650 Park Tower Drive, Suite 800, Vienna, VA 22180
103-104. Office of Scientific and Technical Information, U.S. Department of Energy, P.O. Box 62, Oak Ridge, TN 37831
105. Office of the Assistant Manager for Energy Research and Development, Department of Energy Oak Ridge Operations (DOE-ORO), P.O. Box 2008, Oak Ridge, TN 37831
106. C. E. Olson, Sandia National Laboratories, P.O. Box 5800, Div. 6631, MS 0715, Albuquerque, NM 87185-0716
107. N. Osgood, U.S. Nuclear Regulatory Commission, Office of Nuclear Materials Safety and Safeguards, TWFN 8F5, Washington, DC 20555
108. O. Ozer, Electric Power Research Institute, 3412 Hillview Ave., Palo Alto, CA 94304
109. P. Pacquin, General Nuclear Systems, Inc., 220 Stoneridge Dr., Columbia, SC 29210
110. T. Parish, Department of Nuclear Engineering, Texas A & M University, College Station, TX 77843-3313
111-113. M. Rahimi, 2650 Park Tower Drive, Suite 800, Vienna, VA 22180
114. B. Rasmussen, Duke Power Co., P.O. Box 33189, Charlotte, NC 28242
115. T. L. Sanders, Sandia National Laboratories, P.O. Box 5800, Div. 6609, MS 0720, Albuquerque, NM 87185-0716
116. K. D. Seager, Sandia National Laboratories, P.O. Box 5800, Div. 6643, MS 0716, Albuquerque, NM 87185-0716
117. M. Smith, U.S. Department of Energy, Yucca Mountain Project Office, 101 Convention Center Dr., Las Vegas, NV 89190
118. M. Smith, Virginia Power Co., P.O. Box 2666, Richmond, VA 23261
119. K. B. Sorenson, Sandia National Laboratories, P.O. Box 5800, Div. 6643, MS 0716, Albuquerque, NM 87185-0716
120. F. C. Sturz, Office of Nuclear Material Safety & Safeguards, U.S. Nuclear Regulatory Commission, MS TWFN 8F5, Washington, DC 20555
121. J. Sun, Florida Power & Light Co., P.O. Box 029100, Miami, FL 33102
122. T. Suto, Power Reactor and Nuclear Fuel Development Corp., 1-9-13, Akasaka, Minato-Ku,, Tokyo, Japan
123. R. J. Talbert, Battelle Pacific Northwest Laboratory, P.O. Box 999, Richland, WA 99352
124. T. Taylor, INEL, P.O. Box 4000, MS 3428, Idaho Falls, ID 83403
125. B. Thomas, VECTRA Technologies, Inc., 6203 San Ignacio Ave., Suite 100, San Jose, CA 95119
126. D. A. Thomas, B&W Fuel Co., 101 Convention Center Drive, Suite 527, MS 423, Las Vegas, NV 89109
127. J. R. Thornton, TRW Enviornmental Safety Systems, 2650 Park Tower Dr., Suite 800, Vienna, VA 22180
128. G. Walden, Duke Power Co., P.O. Box 33189, Charlotte, NC 28242
129. M. E. Wangler, U.S. Department of Energy, EH-33.2, Washington, DC 20585-0002
130. R. Weller, U.S. Nuclear Regulatory Commission, TWFN 7J9, Washington, DC 20555
131. A. Wells, 2846 Peachtree Walk, Duluth, GA 30136
132. W. Weyer, Wissenschaftlich-Technische Ingenieurberatung GMBH, Mozartstrasse 13, 5177 Titz-Rodingen, Federal Republic of Germany
133. B. H. White, Office of Nuclear Material Safety & Safeguards, U.S. Nuclear Regulatory Commission, MS TWFN 8F5, Washington, DC 20555
134. J. Williams, Office of Civilian Radioactive Waste Management, U.S. Department of Energy, RW-46, Washington, DC 20545
135. M. L. Williams, LSU Nuclear Science Center, Baton Rouge, LA 70803

136. C. J. Withee, Office of Nuclear Material Safety & Safeguards, U.S. Nuclear Regulatory Commission, MS TWFN 8F5, Washington, DC 20555
137. R. Yang, Electric Power Research Institute, 3412 Hillview Ave., Palo Alto, CA 94304